

Geometrical condition for observing Talbot effect in plasmonics infinite metallic groove arrays

Afshari-Bavil Mehdi, Xiao-Ping Lou(娄小平), Ming-Li Dong(董明利), Chuan-Bo Li(李传波), Shuai Feng(冯帅), Parsa Saviz, Lian-Qing Zhu(祝连庆)

Citation: Chin. Phys. B . 2018, 27(12): 124204. **doi:** 10.1088/1674-1056/27/12/124204
Journal homepage: http://cpb.iphy.ac.cn; http://iopscience.iop.org/cpb

What follows is a list of articles you may be interested in

Surface plasmon polariton at the interface of dielectric and graphene medium using Kerr effect

Bakhtawar, Muhammad Haneef, B A Bacha, H Khan, M Atif

Chin. Phys. B . 2018, 27(11): 114215. **doi:** 10.1088/1674-1056/27/11/114215

Surface plasmon polariton nanolasers: Coherent light sources for new applications

Yu-Hsun Chou(周昱薰), Chia-Jui Chang(張家睿), Tzy-Rong Lin(林資榕), Tien-Chang Lu(盧廷昌)

Chin. Phys. B . 2018, 27(11): 114208. **doi:** 10.1088/1674-1056/27/11/114208

Surface plasmon polariton waveguides with subwavelength confinement

Longkun Yang(杨龙坤), Pan Li(李盼), Hancong Wang(汪涵聪), Zhipeng Li(李志鹏)

Chin. Phys. B . 2018, 27(9): 094216. **doi:** 10.1088/1674-1056/27/9/094216

Plasmonically induced reflection in metal-insulator-metal waveguides with two silver baffles coupled square ring resonator

Zhi-Dong Zhang(张志东), Lian-Jun Ma(马连俊), Fei Gao(高飞), Yan-Jun Zhang(张彦军), Jun Tang(唐军), Hui-Liang Cao(曹慧亮), Bin-Zhen Zhang(张斌珍), Ji-Cheng Wang(王继成), Shu-Bin Yan(闫树斌), Chen-Yang Xue(薛晨阳)

Chin. Phys. B . 2017, 26(12): 124212. **doi:** 10.1088/1674-1056/26/12/124212

A novel phase-sensitive scanning near-field optical microscope

Wu Xiao-Yu, Sun Lin, Tan Qiao-Feng, Wang Jia

Chin. Phys. B . 2015, 24(5): 054204. **doi:** 10.1088/1674-1056/24/5/054204

Geometrical condition for observing Talbot effect in plasmonics infinite metallic groove arrays*

Afshari-Bavil Mehdi[1,2,†], Xiao-Ping Lou(娄小平)[1,2], Ming-Li Dong(董明利)[1,2], Chuan-Bo Li(李传波)[3,‡], Shuai Feng(冯帅)[3], Parsa Saviz[4], and Lian-Qing Zhu(祝连庆)[1,2]

[1] *Joint International Research Laboratory of Advanced Photonics and Electronics, Beijing Information Science and Technology University, Beijing* 100192, *China*

[2] *Beijing Key Laboratory for Optoelectronic Measurement Technology, Beijing Information Science and Technology University, Beijing* 100192, *China*

[3] *School of Science, Minzu University of China, Beijing* 100081, *China*

[4] *Institute of Semiconductors, Chinese Academy of Science, Beijing* 100083, *China*

(Received 15 May 2018; revised manuscript received 24 August 2018; published online 10 November 2018)

The plasmonics Talbot effect in metallic layer with infinite periodic grooves is presented in this study. Numerical approach based on the finite element method is employed to verify the derived Talbot carpet on the non-illumination side. The groove depth is less than the metallic layer thickness; however, for specific conditions, surface plasmons polaritons (SPPs) can penetrate through grooves, propagate under the metallic layer, and form Talbot revivals. The geometrical parameters are specified via groove width, gap size, period, and wavelength, and their proper values are determined by introducing two opening ratio parameters. To quantitatively compare different Talbot carpets, we introduce new parameters such as R-square that characterizes the periodicity of Talbot images. The higher the R-square of a carpet, the more coincident with non-paraxial approximation the Talbot distance becomes. We believe that our results can help to understand the nature of SPPs and also contribute to exploring this phenomenon in Talbot-image-based applications, including imaging, optical systems, and measurements.

Keywords: Talbot image, surface plasmon polaritons, groove array

PACS: 42.30.–d, 78.68.+m, 68.47.De **DOI:** 10.1088/1674-1056/27/12/124204

1. Introduction

The Talbot effect was discovered in 1836. The Talbot effect reveals the appearance of periodic images at serial distances on the back side of a periodic hole and slit array or on the illumination side of a grating when a structure is illuminated by normal monochromatic light.[1] The effect is attributed to nearfield diffraction and has been used in numerous fields, such as acoustics,[2] optical dispersive fiber system,[3] scanning electron microscope imaging,[4] lithography,[5] nonlinear optics,[6] microlens,[7] interferometric measurement,[8] array illumination,[9] and optical trapping.[10]

The unique features of surface plasmon polaritons (SPPs) make them a critical candidate for nanophotonics applications.[11–15] By analogy of SPPs, which are electromagnetic waves propagating along the interface between metal and dielectric, with other electromagnetic waves, we anticipate that SPPs also exhibit periodical revivals. More recently, the formation of revivals in the near field has been explored theoretically[16–20] and experimentally.[21–24] Plasmonics revivals were formed when the light wavelength was smaller than the array period.[25] In addition, their fast damping shortened their propagation length; thus, only the first and second row of Talbot revivals have received the attention. However, the Talbot distance in the plasmonics regime, was not coincident with that in the paraxial approximation that had been introduced by Rayleigh.[26] Furthermore, Oosten *et al.* introduced an alternative approach[22] and derived a non-paraxial formula to explain the shift.

In this paper, we utilize the tunneling nature of SPPs in a periodic groove array and prove that the Talbot carpet can be created if the separation distance is less than the SPPs penetration depth.[27] We use the finite elements method (FEM)-based numerical approach and determine the geometrical criteria for observing revivals. To achieve this goal, two ratios relating to geometrical parameters are introduced and a proper set of values is determined for each ratio. The comparison is accomplished by using the *R*-square, which is a fitting value in the MATLAB fitting tool. Furthermore, the contrast and size of self-images are determined. Our data will improve the understanding of SP tunneling in groove-array structure that can be used in a wide range of applications, such as in nanolithography, nonlinear optics, and image processing.

*Project supported by the 111 Project, China (Grant No. D17021) and the Changjiang Scholars and Innovative Research Team in University, China (Grant No. PCSIRT, IRT_16R07).

†Corresponding author. E-mail: mehdi.afshari@bistu.edu.cn

‡Corresponding author. E-mail: cbli@semi.ac.cn

© 2018 Chinese Physical Society and IOP Publishing Ltd

2. Structure description and simulation set up

Figure 1 shows a schematic view of the proposed infinite periodic groove array drilled on a silver film. To excite SPPs, the TM mode light is incident from the top, where it is normalized into unity. P, d, H, and W denote period, groove width, step thickness, and film thickness, respectively.

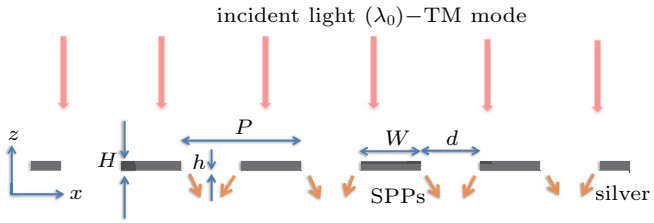


Fig. 1. (color online) Two-dimensional scheme of proposed infinite periodic groove array structure.

Our simulation approach is based on FEM and we used the Comsol commercial simulation platform. The boundary condition for the top and bottom were scattering boundary conditions that for normal illumination are proper conditions, whereas we used the periodic condition at each of the side boundaries. The silver dielectric function was described by Drude model ($\varepsilon_m = \varepsilon_\infty - \omega_p^2/(\omega^2 + i\omega\gamma)$), where ε_∞ (high-frequency bulk permittivity) is 4.2, ω_p (the bulk plasmon frequency) is 1.346×10^{16} rad/s, and γ (the electron collision frequency) is 9.617×10^{13} rad/s.[28] Moreover $\omega = 2\pi c/\lambda$, where c and λ denote the light speed and incident wavelength that was fixed at 632.8 nm. The mesh size inside the grooves and the gap were both considered to be 5 nm, whereas in the rest of area it was 20 nm. The goal was to determine the proper value for h, W, P, and d. To achieve this goal, in the way similar to that in Ref. [21] we introduced two "opening" ratios α and γ, where α is d/P and γ is P/λ. The presence of grooves can provide the necessary wave vector to excite the SPPs dependent on geometrical parameter and incident light wavelength. We set the structure parameters to be $H = 150$ nm, $h = 20$ nm, $P = 1220$ nm, and $\alpha = 0.5$, which lead to $W = d = 610$ nm. Our proposed configuration was a broadband device[29] in the visible range. However, at a wavelength of 632.8 nm, the transmission was higher.

3. Results and discussion

Two basic characteristics of SPPs are its propagation length, expressed by $L_{sp} = 1/\mathrm{Im}(2k_{sp})$, where $k_{sp} = 2\pi/\lambda_{sp}$, $\lambda_{sp} = \lambda_0\sqrt{((\varepsilon_m+1)/\varepsilon_m)}$, and penetration depth, expressed by[27] $\lambda/2\pi\sqrt{|\varepsilon_m|}$. To design plasmonic devices, these characteristics should be considered accordingly. The SPPs can tunnel through metallic layer if the thickness is less than the penetration depth. For silver at this wavelength, the penetration is 25 nm; thus, h should be less than this value. Furthermore, SP decays rapidly after propagation length; thus, for any application the effective working length should be less than this value. For silver at this wavelength, the propagation length is 36 μm; thus, only the revivals formed in this length have sufficient intensity. Figure 2(a) shows the electric field spectra in a logarithmic scale when the above criteria are considered. Talbot revivals and fractional revivals both can be observed. Lines A and B represent the non-paraxial and paraxial prediction value for Talbot distance, respectively. Line A (the first Talbot revival), which is located at 4.36 μm, is more coincident with simulation results; thus, the non-paraxial approximation that is expressed by[22]

$$\tau = \lambda_{SPP}/\{1 - [1(\lambda_{SPP}/d)^2]^{1/2}\} \quad (1)$$

is a preferable formula. The light intensity profile along the z direction in the center of the structure has a periodic behavior where the peaks correspond to Talbot revivals. To find the optimized geometrical parameters, we introduce physical parameters. R-square is the fitting value for estimating the wave periodicity and is based on Fourier series fitting tool in MATLAB. Size (along x direction at first revival) is defined as the width cut by the middle intensity line located between the peak and

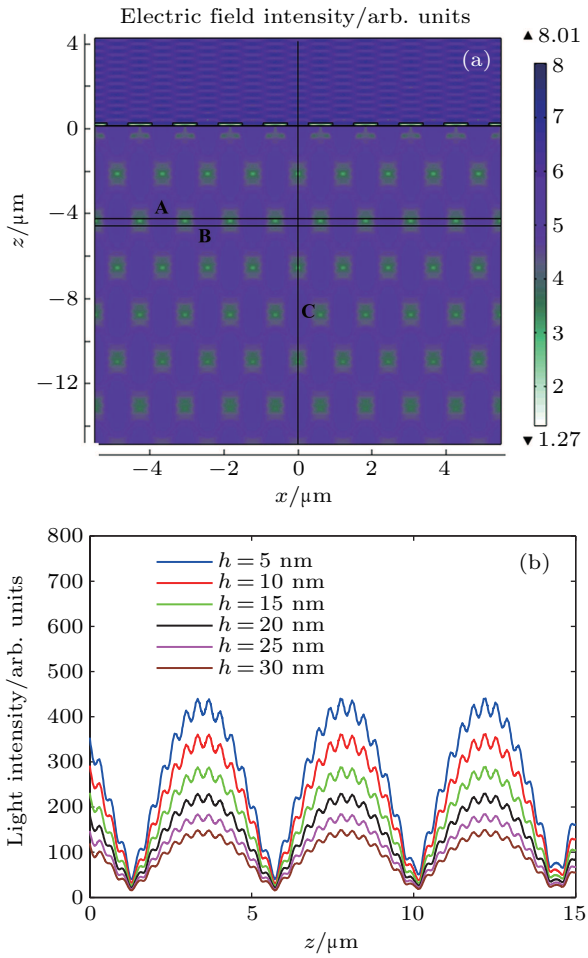


Fig. 2. (color online) (a) Electric field spectrum of the proposed structure. Talbot images are created on non-illumination side, with incident wavelength being 632.8 nm, and geometrical parameters being set to be $H = 150$ nm, $h = 20$ nm, $P = 1220$ nm, and $\alpha = 0.5$. (b) Plots of light intensity versus z for different gap thickness.

minimum on the intensity profile. Contrast is defined as the difference between the peak and minimum of intensity over the peak value multiplied by 100. Favorable Talbot revivals should have a smaller full width at half maximum (FWHM) and higher *R*-square and contrast.[29] Meanwhile, the revivals with sizes closer to the actual groove size are better.

The intensity profiles for different gaps are indicated in Fig. 2(b). It can be seen that Talbot distance does not change but the intensity drops rapidly with increasing h. Figure 3(a) shows the contrast variation with gap thickness, when gap equals 15 nm, the contrast is highest. The revival size is enhanced smoothly as shown in Fig. 3(b). The *R*-square profile, depicted in Fig. 3(c), has the highest value corresponds to h equal to 15 nm. The peak value of light intensity drops sharply as indicated in Fig. 3(d). It can be concluded that better Talbot revivals are formed when the gap is a value between 15 nm and 20 nm.

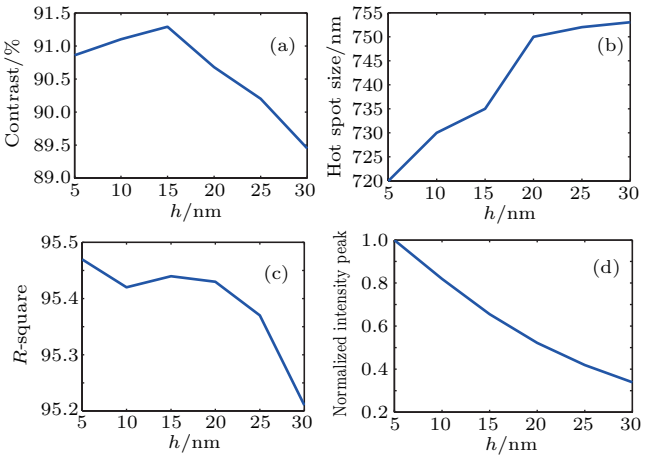


Fig. 3. (color online) (a) Contrast, (b) revival size, (c) *R*-square, and (d) intensity peak versus gap thickness.

4. Discussion on geometrical parameters

To gain a more in-depth insight into the geometrical parameter criteria, we investigate the physical parameter variations for different values of α and γ. This is similar to the approach previously presented by Hua *et al.* for the nanohole array.[30] We are interested in determining the effective working range for geometrical parameters of the groove array. Three parameters, namely, P, λ, and α, are subjected to optimization. Three different cases are considered:

4.1. Case 1 where *P* and λ are fixed and α is varying

Since period is constant, any change of α value can cause the thickness of grooves and steps to be modified. The value of P and λ are set to be 1220 nm and 632.8 nm, respectively. The light intensity along the central line varying with position in the z direction for α value increasing from 0.2 to 0.7 is shown in Fig. 4(a). From Eq. (1), the locations of revivals are irrelevant to α variation. However, a slight shift in Talbot distance is observed in simulation results. It is found that when α is located between 0.5 and 0.58, the non-paraxial approximation is well coincident. Figure 4(b) shows the peak intensity variation with α, indicating that lower α can lead the light intensity to reach the highest value. However, from Fig. 4(c) we can see that for lower α the contrast is very low, while for α in a range between 0.45 and 0.6 the contrast is sufficiently high. Figure 4(d) shows that in the *R*-square profile, for the narrow range between 0. 5 and 0.58, the *R*-square is nearly constant and stable. We can generalize that the interval between 0.5 and 0.58 is a stable working zone, and any value located in this range can give proper Talbot image with high contrast, *R*-square, and intensity.

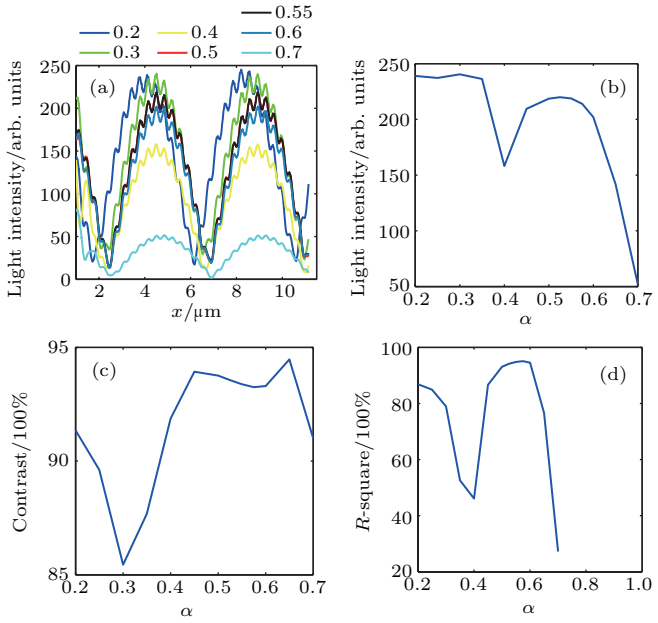


Fig. 4. (color online) (a) Plots of light intensity versus x in center of structure for different values of α. (b) Peak intensity, (c) contrast, and (d) *R*-square varying with α.

4.2. Case 2, where λ is fixed and *P* is varying

The wavelength is still set to the same value as used previously. For each P, proper α should be determined. Moreover, it is found that light intensity profile behaves differently for various γ values. Figure 5 shows the light intensity profiles for four γ values for some α values ranging from 0.3 to 0.7. According to the result of the light intensity profile, three different regimes are recognized:

Regime 1 $\gamma \leq 1.25$ and $\gamma \geq 2$: Talbot image is not formed; thus, we ignore the studying of these values. When $\gamma = 2$ for small values of α, Talbot revivals do not appear. However, for the sake of compression, we assume the location of maximum intensity to be the revival point and extract the data.

Regime 2 $1.25 < \gamma < 1.7$, and $1.95 < \gamma < 2$: despite the fact that the Talbot revivals appear, the *R*-square is less than 90%, or the Talbot distance is not consistent with the non-paraxial approximation. We only study the profiles with *R*-square larger than 90% to guarantee that their Talbot patterns are satisfactory.

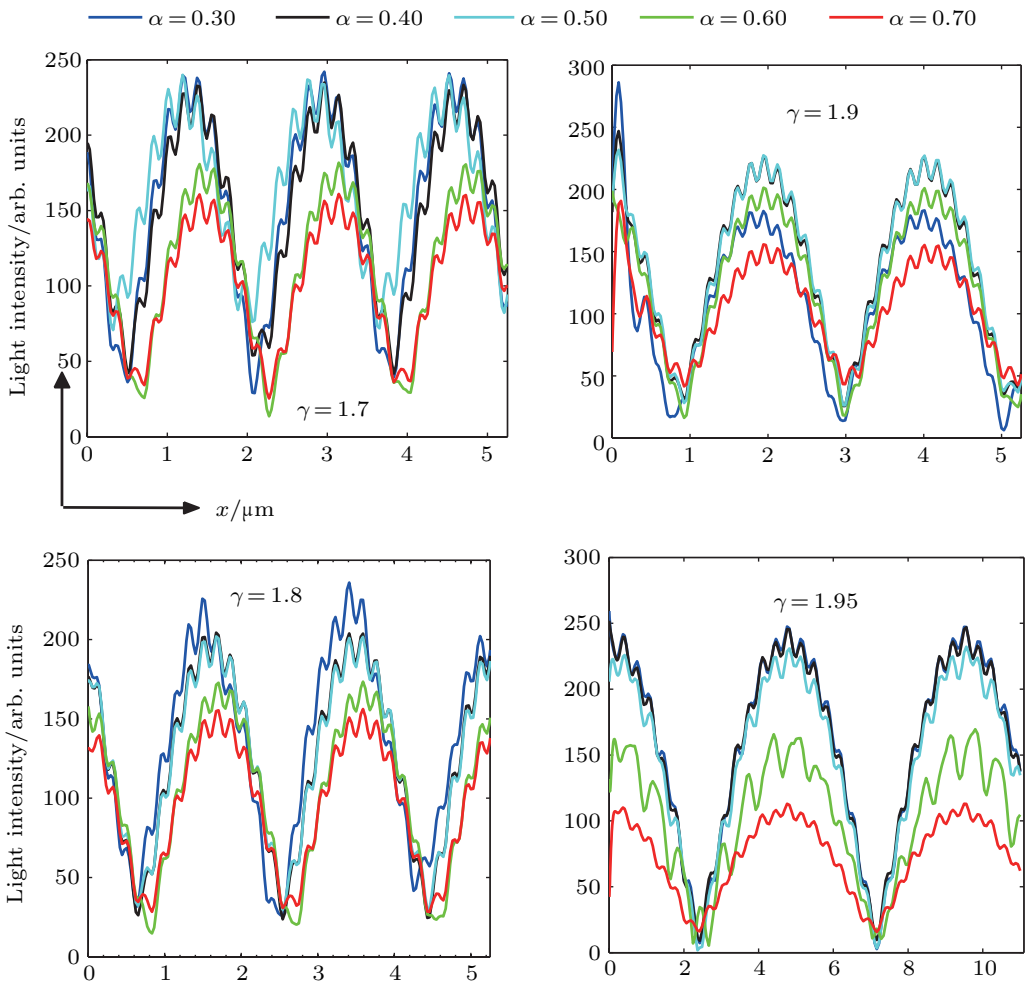


Fig. 5. (color online) Light intensity profiles for different γ values while in each period α changes. In each period, some values of α show proper periodic profiles; however, for any desired period, α values located between 0.5 and 0.58 provide appropriate Talbot revivals.

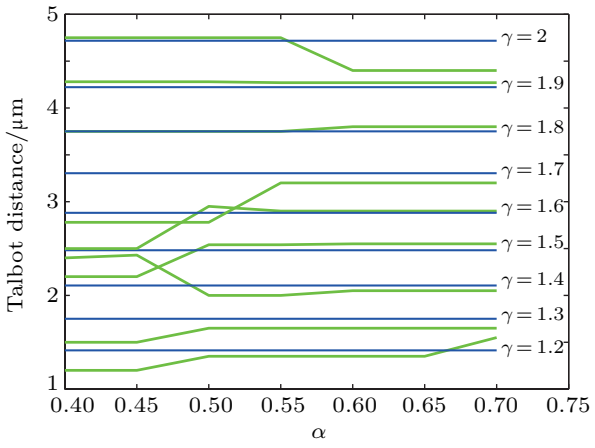


Fig. 6. (color online) Plots of Talbot distance versus α for various values of opening ratio γ. Blue and green lines represent the non-paraxial approximation and numerical result, respectively.

Figure 6 shows Talbot distance variations versus α for various γ values. By changing γ, the periods change; therefore, Talbot distances vary accordingly. For each γ, a slight discrepancy exists between theory and simulation, which is probably attributed to the difference in the nature of diffraction effect between the grating and groove structure. It is observed that for α located in a middle range, any γ can approximately form Talbot revivals at the predicted location. It can be concluded that for α values located in a range from 0.5 to 0.58 similar to the scenario in Subsection 4.1, better periodic behavior and high compatibility with non-paraxial approximation can be obtained.

Regime 3 $1.7 < \gamma < 1.95$: we refer to this range as working zone; because the profiles have an apparent periodic behavior and appeared Talbot images are in good consistency with non-paraxial approximation. The plots of R-square versus α for different γ values are shown in Fig. 7(a), whereas the plots of R-square versus γ for different α values are given in Fig. 7(b). Through these two figures, we can completely determine the working zones, respectively, for α and γ. The hatched sections represent working zones, respectively, for α and γ. The working zone for α is still the same as that in regime 1. Generally speaking, for this wavelength, opening ratios located within the hatched areas both give the distinguished Talbot carpet.

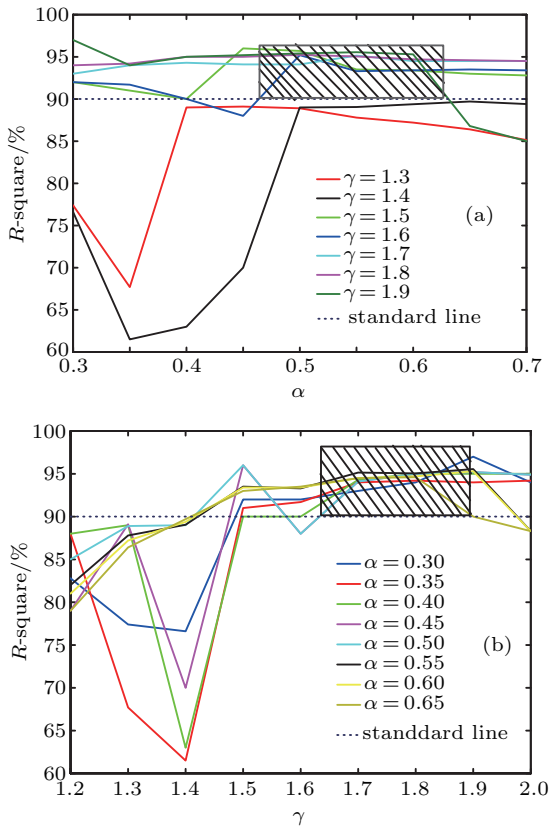


Fig. 7. (color online) (a) Plots of R-square versus α for different γ values, and (b) plots of R-square versus γ for different α values. Hatched rectangles represent working zones for α and γ, respectively.

4.3. Case 3, where λ and P are both varying

For each wavelength, the proper γ and α should be recognized. However, to avoid long simulation time and large memory space and to accelerate the simulation speed, some approximations are indispensable. In the previous parts we found that for different cases, α has a constant working zone; thus, in this regime we pick up the best value for α, which is 0.54, and set it to be a constant. Figure 8 shows the light intensity profiles versus γ for different wavelengths within the visible range. As shown in the figure, the intensity magnitudes are different at various wavelengths, which can be attributed to the transmission variation due to mismatch in wave vector at different wavelengths. Furthermore, the Talbot distance increases with enhancing the wavelength, which is in good agreement with Eq. (1). The scenarios for four wavelengths are presented, and more details can be found through the legend. Different colors represent different opening ratio γ values. A smaller γ does not apparently represent highly standard periodic behavior; meanwhile the light intensity is not high. Like the previous parts, we can define three regimes based on the γ value for each wavelength:

Regime 1 $\gamma \leq 1.25$ and ≥ 2: our results show that the Talbot image does not appear any more.

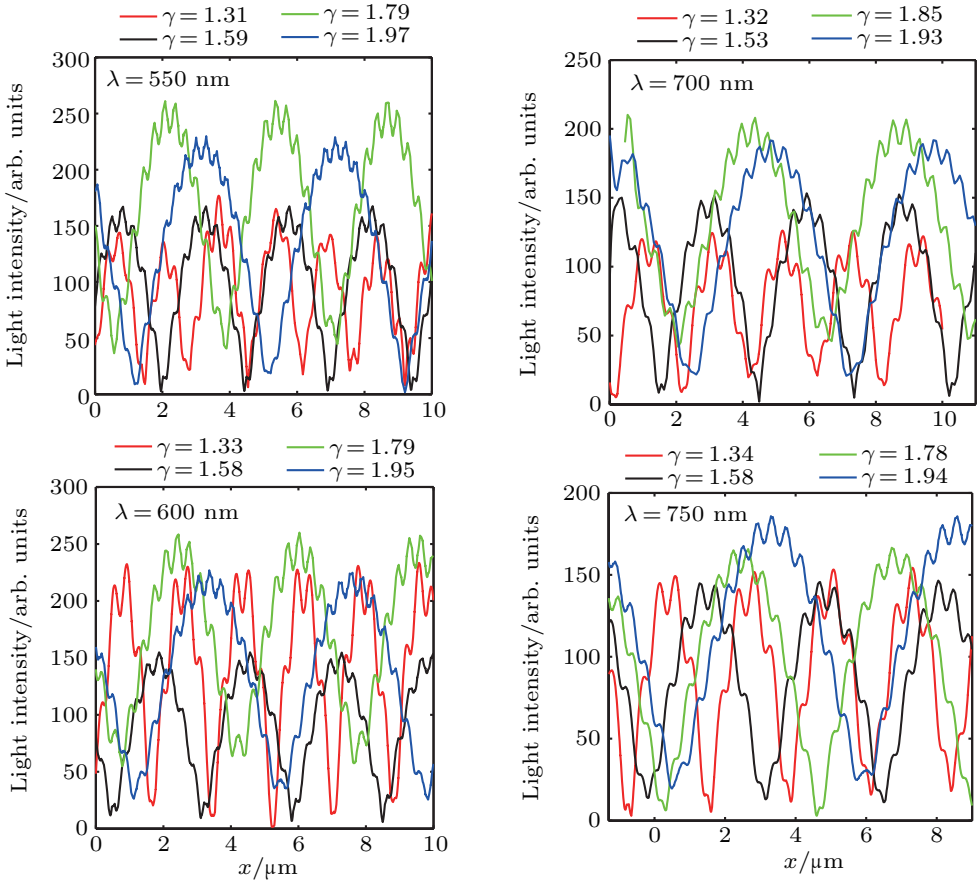


Fig. 8. (color online) Light intensity profiles for different wavelengths, with α fixed but γ varied.

Regime 2 $1.25 < \gamma < 1.58$: $1.97 < \gamma < 2$: The Talbot revivals are formed but R-square is less than 90% and Talbot distance does not accord with non-paraxial predictions.

Regime 3 $1.58 < \gamma < 1.97$: The Talbot images are created with R-square is larger than 90%. Figure 9 shows the plots of the Talbot distance location versus opening ratio γ for different wavelengths. The rectangles show the areas where simulation results are in sufficiently good agreement with theoretical results. The rectangles do not overlap with each other, which makes it difficult to determine the working zone. It is concluded that for different wavelengths, simulation-based and analytical-based Talbot distances are not well coincident with each other. To determine the working zone, the R-square variations are required.

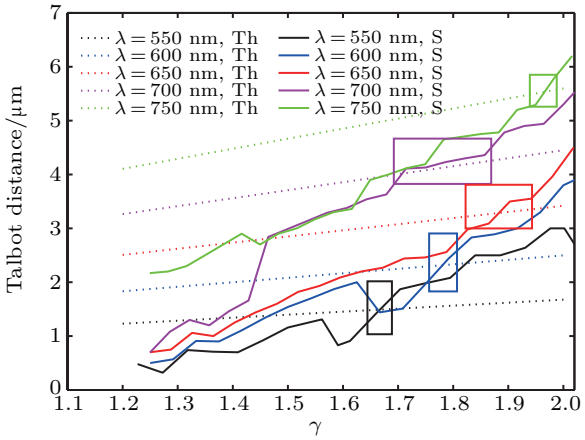


Fig. 9. (color online) Numerical and theoretical results of Talbot distance varying versus γ for different wavelengths.

The results are shown in Fig. 10. It is observed that within the hatched area where γ is between 1.58 and 1.97, the R-square is sufficiently high, and we can refer to it as a working zone. Generally speaking, by implementing the result of the previous parts, we can summarize that for any wavelength under any condition, the working zones for γ and α to achieve a preferred Talbot carpet should be between 1.7 and 1.95 and between 0.5 and 0.58, respectively.

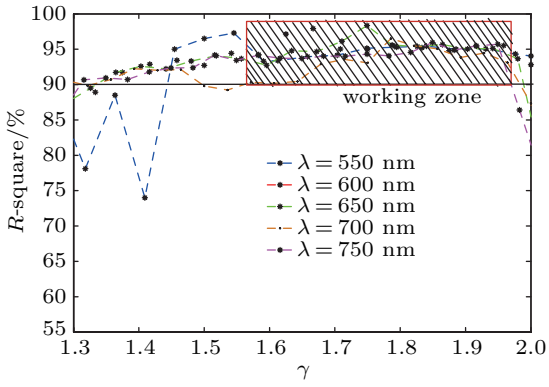


Fig. 10. (color online) Plots of R-square versus γ for different wavelengths, where Hatched rectangle located between 1.58 and 1.97 represents working zone.

5. Conclusions and perspectives

In this work, the geometrical parameter criteria for observing the Talbot effect in plasmonic infinite periodic metallic groove arrays are determined and analyzed numerically. Two opening ratios are introduced to investigate the structure. Furthermore, the R-square, size, and contrast for revivals are determined as well. Three different cases are imagined. For any wavelength in the visible range, the opening ratio α has a working zone located between 0.5 and 0.58. Meanwhile, the opening ratio γ has a working zone located between 1.7 and 1.95. In this range, the Talbot revivals with high contrast and R-square appear. Additionally, their Talbot distances are in good agreement with non-paraxial approximation. Our result can directly have the Talbot-image based applications, especially in imaging and lithography.

References

[1] Talbot H F 1836 *London Edinburgh Philos. Mag. J. Sci.* **9** 401
[2] Zhu H and Semperlotti F 2015 *Phys. Rev. B* **91** 104304
[3] Azaña J 2005 *Opt. Lett.* **30** 227
[4] Kim H, Li W, Danylyuk S, Brocklesby W S, Marconi M C and Juschkin L 2015 *J. Phys. D. Appl. Phys.* **48** 375101
[5] Stuerzebecher L, Harzendorf T, Vogler U, Zeitner U D and Voelkel R 2010 *Opt. Express* **18** 19485
[6] Liu D, Zhang Y, Wen J, Chen Z, Wei D, Hu X,Zhao G, Zhu S N and Xiao M 2015 *Sci. Rep.* **4** 6134
[7] Gao H, Hyun J K, Lee M H, Yang J C, Lauhon L J and Odom T W 2010 *Nano Lett.* **10** 4111
[8] Liu L 1989 *Appl. Opt.* **28** 4668
[9] Maddaloni P, Paturzo M, Ferraro P, Malara P, De Natale P, Gioffrè M, Coppola G and Iodice M 2009 *Appl. Phys. Lett.* **94** 121105
[10] Song Y G, Han B M and Chang S 2001 *Opt. Commun.* **198** 7
[11] Ao Z G, Sun J H, Cai H, Song G F, Song J K, Song Y Z and Xu Y 2016 *J. Semicond.* **37** 123002
[12] Zhang Z Y and Song G F 2017 *J. Semicond.* **38** 22001
[13] Bavil M A, Deng Q and Zhou Z 2014 *Opt. Lett.* **39** 4506
[14] Bavil M A, Zhou Z and Deng Q 2013 *Opt. Express* **21** 17066
[15] Bavil M A, Liu Z, Zhou W, Li C and Cheng B 2017 *Plasmonics* **12** 1709
[16] Cherukulappurath S, Heinis D, Cesario J, van Hulst N F, Enoch S and Quidant R 2009 *Opt. Express* **17** 23772
[17] Li L, Fu Y, Wu H, Zheng L, Zhang H, Lu Z, Sun Q and Yu W 2011 *Opt. Express* **19** 19365
[18] Maradudin A A and Leskova T A 2009 *New J. Phys.* **11** 33004
[19] Cortés L R, Chatellus H G and Azaña J 2016 *Opt. Lett.* **41** 340
[20] Shi X, Yang W, Xing H and Chen X 2015 *Opt. Lett.* **40** 1635
[21] Zhang W, Zhao C, Wang J and Zhang J 2009 *Opt. Express* **17** 19757
[22] Van Oosten D, Spasenović M and Kuipers L 2010 *Nano Lett.* **10** 286
[23] Chowdhury M H, Lindquist N C, Lesuffleur A, Oh S H, Lakowicz J R and Ray K 2012 *J. Phys. Chem. C* **116** 19958
[24] Yu Y, Chassaing D, Scherer T, Landenberger B and Zappe H 2013 *Plasmonics* **8** 723
[25] Li W, Li H, Gao B and Yu Y 2017 *Sci. Rep.* **7** 45573
[26] Rayleigh L 1881 *London Edinburgh Dublin Philos. Mag. J. Sci.* **11** 196
[27] Maier S A 2007 *Plasmonics: Fundamentals and Applications* (Springer Science & Business Media) p. 28
[28] Palik E D 1998 *Handbook of Optical Constants of Solids* (Academic Press)
[29] AfshariBavil M, Luo X P, Li C B, Feng S, Dong M L and Zhu L Q 2018 *Plasmonics*
[30] Hua Y, Suh J Y, Zhou W, Huntington M D and Odom T W 2012 *Opt. Express* **20** 14284